

# Advances in electrical impedance methods in medical diagnostics

A. NOWAKOWSKI<sup>1\*</sup>, T. PALKO<sup>2</sup>, and J. WTOREK<sup>1</sup>

<sup>1</sup>Department of Biomedical Engineering, Gdańsk University of Technology, 11/12 Narutowicza Str., 80-952 Gdańsk, Poland

<sup>2</sup>Institute of Precision and Biomedical Engineering, Warsaw University of Technology, 8 Św. A. Boboli Str., 02-525 Warsaw, Poland

**Abstract.** The electrical impedance diagnostic methods and instrumentation developed at the Gdańsk and Warsaw Universities of Technology are described. On the basis of knowledge of their features, several original approaches to the broad field of electrical impedance applications are discussed. Analysis of electrical field distribution after external excitation, including electrode impedance, is of primary importance for measurement accuracy and determining the properties of the structures tested.

Firstly, the problem of electrical tissue properties is discussed. Particular cells are specified for *in vitro* and *in vivo* measurements and for impedance spectrometry. Of especial importance are the findings concerning the electrical properties of breast cancer, muscle anisotropy and the properties of heart tissue and flowing blood. The applications are both important and wide-ranging but, for the present, special attention has been focused on the evaluation of cardiosurgical interventions.

Secondly, methods of instrument construction are presented which use an electrical change in conductance, such as impedance pletysmography and cardiography, for the examination of total systemic blood flow. A new method for the study of right pulmonary artery blood flow is also introduced. The basic applications cover examination of the mechanical activity of the heart and evaluation of many haemodynamic parameters related to this. Understanding the features that occur during blood flow is of major importance for the proper interpretation of measurement data.

Thirdly, the development of electrical impedance tomography (EIT) is traced for the purposes of determining the internal structure of organs within the broad field of 2-D and 3-D analysis and including modelling of the organs being tested, the development of reconstruction algorithms and the construction of hardware.

**Key words:** electrical impedance, tissue characterisation, spectrometry, cardiography, pletysmography, hypoxaemia, tomography.

## 1. Introduction

Access to up-to-date information on advances in the field of electrical bio-impedance (EBI) research is relatively easy thanks to regular conferences such as the International Conference of Electrical Bio-Impedance ICEBI, which has been held since 1969. It is important here to mention conferences at which Polish groups have been well represented, such as that held in Heidelberg in 1995 [1], in Barcelona in 1998 [2], in Oslo in 2001 [3] and the recent 12<sup>th</sup> ICEBI and 5<sup>th</sup> Electrical Impedance Tomography Conference (EITC) held in Gdańsk in 2004 [4] – <http://icebi.gda.pl>. There are also specialised publications such as [5–7] or special issues of journals such as [8]. In addition to these there is an internet service devoted to EI mailing list members – <http://www.eit.org.uk>, as well as the homepage of the International Society of Electrical Bio-Impedance (ISEBI) – <http://www.isebi.org>. A number of other specific original and review publications such as [9–11] deal with recent research in this field. In Poland the research groups in Gdańsk and Warsaw, which work in close collaboration (<http://www.eti.pg.gda.pl/katedry/kib/>) and (<http://ipib.mech.pw.edu.pl/>), are the most active in EI. The recent research results of these two groups are discussed in the following text.

Since the 1930s basic electrical impedance measurements in biology have been well known. From the late 1970s onwards electrical impedance tomography (EIT) has also been regarded as a promising technology in medical applications. The technology is non-invasive and measurements that are based on current or voltage excitation do not appear to be technically difficult, making the instrumentation relatively inexpensive. However, the clinical applications of EI methods are still not as popular as one might expect, taking into account the years of research behind them. The main reason for this is a lack of confidence in diagnostic data based on indirect measurements of limited accuracy and with the rather low resolution of the methods known to date. Today, therefore, research efforts are concentrating on methods of increasing accuracy, on gaining a proper understanding of existing features and on improving the numerical models of the objects tested, which is important for data interpretation.

Applications that are already accepted in clinics include the use of electrical impedance (EI) measurements in functional studies of the heart and the cardiovascular system such as impedance cardiography (ICG), in examination of the digestive system and in monitoring of the respiratory system. The clinical applications of EIT have also been known for several years [1–8].

\*e-mail: antowak@biomed.eti.pg.gda.pl

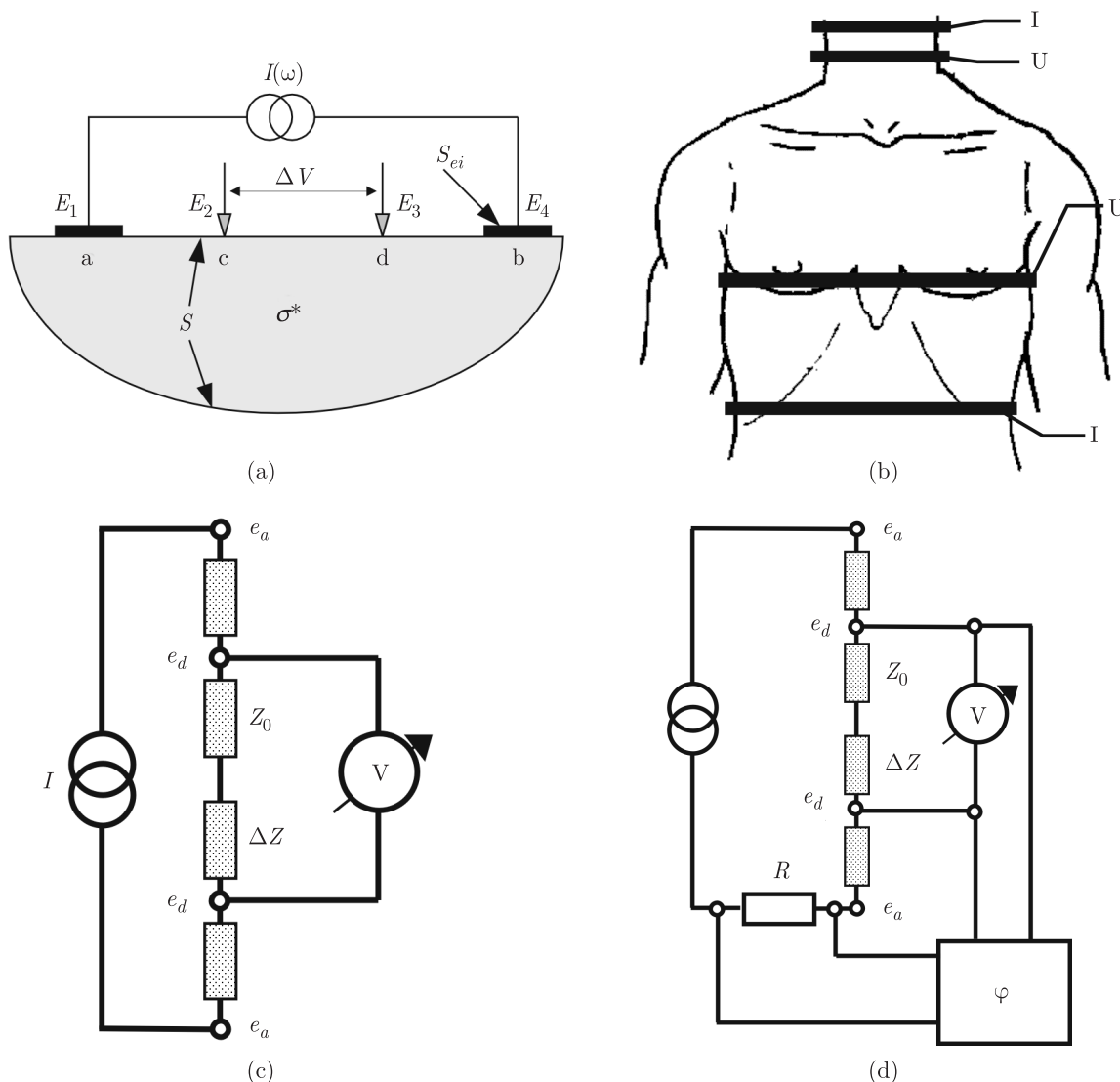


Fig. 1. Tetra-polar configuration of electrodes,  $S$  boundary of the object,  $S_{ei}$  – electrode surface; b) The ICG electrodes, Kubicek configuration; c) Equivalent electrical circuit of the tetra-polar electrode configuration; d) Block diagram of the phase-sensitive measuring set

At present much research effort is being concentrated on cancer detection (mammography) and brain examination. However, in these applications the clinical use of EIT has still not proved very successful, despite the fact that many research groups are deeply involved in the development of measurement instrumentation and appropriate software, including new reconstruction algorithms. In 1999 Siemens marketed TransScan, the first commercially available EI breast cancer diagnostic system, providing simple visualisation of 2-D projections of breast tissue electrical properties. In the USA the Federal Drug Administration approved its use for clinical applications. Recent developments in EIT concern hardware solutions, including multi-frequency measurements, new reconstruction algorithms, and new approaches to non-contact inductive or MRI-EIT based systems have already been presented [4,8]. Presented here are selected clinical applications of impedance pletysmography and cardiography for the study of systemic and pulmonary blood circulation and impedance spectrometry

for characterising hypoxaemic, cancerous or ischemic tissues. Some of the problems associated with EIT development are also discussed.

## 2. Background

Electrical potential distribution in a volumetric conductor is described by Maxwell's equations. This also holds true in the case of biological tissues, which are, in the main, good conductors. Taking into account that the human organism may be regarded as an electrical source-free region, that biological tissues are mainly anisotropic and conductive in character and that magnetic fields can be neglected, the resulting relationship is reduced to the equations:

$$\nabla \cdot \mathbf{j} = 0, \tag{1a}$$

$$\mathbf{j} = \sigma \mathbf{E}, \tag{1b}$$

and

$$\mathbf{E} = -\nabla\phi, \quad (1c)$$

where  $\mathbf{j}$  – current density,  $\mathbf{E}$  – electric field,  $\phi$  – potential,  $\sigma$  – conductivity of a medium (in general it may be a complex number). All quantities are functions of the localisation and frequency of the electrical field. In order to solve equation (1a), boundary conditions dependent on impedance measuring configurations are to be assumed. Tetra-polar measurement systems are mainly used in EI measurements.

The configuration shown in Fig. 1a is typical for EI spectroscopy, cardiography, pletysmography, EIT and other practical applications. In some applications this configuration requires a special construction and placement of the electrodes. For example, in EI cardiography (ICG) the Kubicek configuration [12] with extended four-ring electrodes is usually applied (Fig. 1b). Typical measuring circuits allowing tetra-polar measurements are shown in Figures 1c and 1d. The number of electrodes used depends on the application and may be multiplied, especially in EIT. In order to avoid non-linear effects, a pair of excitation, usually current, electrodes is employed to introduce low-intensity alternative current. The resultant potential is measured by means of a separate pair of voltage electrodes. In this case boundary conditions state that the current flux (density) normal to the outer surface is zero everywhere except for the places where the current electrodes are attached, as is shown by equation (2a):

$$\frac{\partial\phi}{\partial\mathbf{n}} = 0 \quad \text{on} \quad S - S_{ei}. \quad (2a)$$

At the surface of the current electrodes a constant potential is assumed, which is described by the following equation:

$$V = V_{ei} \quad \text{on} \quad S_{ei}, \quad (2b)$$

where  $i$  – number of current electrodes,  $S$  – outer surface of a volumetric conductor,  $S_{ei}$  – surface of the  $i$ -th electrode,  $\mathbf{n}$  – vector normal to  $S$ . Assuming that the voltage electrode is an equipotential surface, the mutual impedance  $Z_t$  is described as:

$$Z_t = \frac{\phi_{CD}}{I_\phi}, \quad (3)$$

where  $\phi_{CD}$  – potential drop between voltage electrodes,  $I_\phi$  – current flowing between current electrodes. When the conductivity distribution changes from  $\sigma(x, y, z)$  to  $\sigma(x, y, z) + \Delta\sigma(x, y, z)$ , the change of the mutual impedance  $\Delta Z_t$  is given by [13]:

$$\begin{aligned} \Delta Z_t = & - \int_V \Delta\sigma(x, y, z) \\ & \times \frac{\nabla\phi(\sigma(x, y, z) + \Delta\sigma(x, y, z))}{I_\phi} \\ & \times \frac{\nabla\psi(\sigma(x, y, z))}{I_\psi} dv, \end{aligned} \quad (4)$$

where  $\psi$  indicates the potential distribution resulting from the current  $I_\psi$  flowing between the current electrodes and  $\phi$  is the hypothetical potential distribution associated with the current flowing between the pair of voltage electrodes. The integration is performed over the volume  $V$ , where the conductivity

change is non-zero;  $\Delta\sigma(x, y, z) \neq 0$ . The potential distribution  $\phi$  is calculated after the change  $\Delta\sigma(x, y, z)$  in the conductivity.  $\nabla\psi/I_\psi = L_\psi$  and  $\nabla\phi/I_\phi = L'_\phi$  are referred to as the lead fields. The superscript  $t$  indicates that the lead field  $L'_\phi$  is evaluated following the change in conductivity. The scalar product of the two lead fields is called the sensitivity function.

The structure tested can be divided into regions of constant conductivity change  $\Delta\sigma(x, y, z)$ , and then equation (4), utilising a property of the integration operator, can be expressed as:

$$\Delta Z_t = \sum_i^N K_i \Delta\sigma_i, \quad (5)$$

where  $K_i$  is given as

$$K_i = - \int_{V_i} L_\psi \cdot L'_\phi dv, \quad (6)$$

where  $\Delta Z_t$  – total impedance change;  $\Delta\sigma_i$  – regional (local) conductivity change;  $N$  – number of regions. Relation (5) allows the separation of  $\Delta Z_t$  into components  $\Delta Z_i$  arising from a chosen region (organ) or phenomenon.

In order to make accurate measurements of electrical conductivity changes in the configurations shown in Figs. 1c and 1d, the following relation (7) between the current sources  $I$  and the measured impedance  $Z_0$  should be fulfilled:

$$\left| \frac{\Delta I}{I} \right| \ll \left| \frac{\Delta Z}{Z_0} \right| \quad (7)$$

Assuming that  $|\Delta Z/Z_0| \cong 0.01$  or less, condition (7) demands a special construction of the current source, ensuring very high output impedance and very low stray capacitance. In practice this is an extremely difficult technical requirement.

Generally, there are several problems related to the measurement hardware. The following list includes only the basic ones:

1. Knowledge of electrical field distribution after excitation. In practice only uniform potential distribution allows accurate data interpretation.
2. The properties of biological tissues, their characterisation and their role in determining the technical data of hardware, especially the use of measurement frequency, and also data interpretation for proper EIT reconstruction algorithms. Interpretation of diagnostic data is related to the models of the tested organs and the measurement applicators.
3. Development of electronic front-ends operating in a broad range of measurement frequencies and the use of very fast data acquisition systems allowing multi-electrode measurements.
4. The influence of electrode impedance, usually unknown, which limits the accuracy of current excitation and that of measurements.
5. The construction of electrodes and measurement limitations in terms of applicable current density and/or voltage amplitudes.
6. Multi-electrode configurations and limitation of electrode number in EIT.

### 3. Impedance spectrometry for tissue characterisation

For the characterisation of tissue spectroscopic studies are performed on the basis of determination of its complex electrical impedance as a function of frequency. The modulus and the phase angle between the excitation current and voltage or the components of resistance and reactance measured over a broad frequency range should be determined. In order to solve the problem of making accurate measurements, special cells for *invitro* and *invivo* measurements are constructed. See, for example, [14–16]. This method enables tissue to be characterised in different states, such as cancer and ischemia, and practically in clinical conditions allows for the examination of body composition and the evaluation of the extracellular and intracellular water ratio in the region of the body under study. In our laboratories special attention is focused on studies concerning the electrical properties of breast cancer, anisotropy of the muscles, the properties of flowing blood and evaluation of cardiosurgical interventions. See, for example, [17–19].

As an example, a special cell construction allowing uniform electrical potential distribution proper for *invitro* measurements is shown in Figs. 2a and 2b [14]. A two-compartment cell, of internal cylindrical and external ring shapes is kept at a constant temperature, typically 37°C. The inner part consists of a chamber and four electrodes ready for tetra-polar measurements. This was applied in making cancer tissue measurements performed within 5 minutes of tissue resection. The results are shown in Fig. 3 for healthy and inter-medium tissue samples and tissue affected by breast cancer [17]. A high phase shift and good conductivity are characteristic for the cancerous tissue.

Another important application of EI measurements is determination of the processes taking place in the heart during cardiosurgical interventions. At the stage of *invivo* experiments on animals (performed according to the legal regulations and with the permission of the local Committee of Ethics in Medicine) the optimised solutions are analysed during, for example, evoked heart stroke, CABG and OP CABG procedures [15,18]. The experiments have been performed using ring electrodes attached to the heart in the region of interest. As an example, the change in time in the blood flow arrest region of a pig heart is envisaged by electrical impedance measurements (Fig. 4a) while the cross-section of the heart with the region of affected tissue is clearly visible (Fig. 4b), as a result of clamping the left descending artery.

Further important conclusions concern the evaluation of blood flow [19,20]. An important change in the electrical properties of flowing and still blood is observed. This is of great importance from the point of view of measurement data interpretation.

The characterisation of ischaemic tissues performed at the Institute of Precision and Biomedical Engineering of Warsaw University of Technology comprise experimental studies and clinical examination of human limb segments. Some of the results of experiments performed on 10 Wistar rats (200–300 g) anaesthetised with sodium pentobarbital at a dose of 10 mg/kg

are discussed briefly here. After tracheotomy the animals were respired artificially with air via a tracheal cannula. Heparin, 2500 i.u., was injected into the left ventricle, the ascending aorta was cut and the cannula was inserted into the aorta above the aortic valve.

An impedance spectrometer based on the tetra-polar current method as developed previously by T. Palko et al., [21] was used for the measurement of the complex impedance (modulus and phase angle) of the isolated rat heart. During the experiment four harpoon-type needle electrodes were applied. One current electrode was fixed in the upper part of the heart and the other in the lower part of the heart. The electrodes

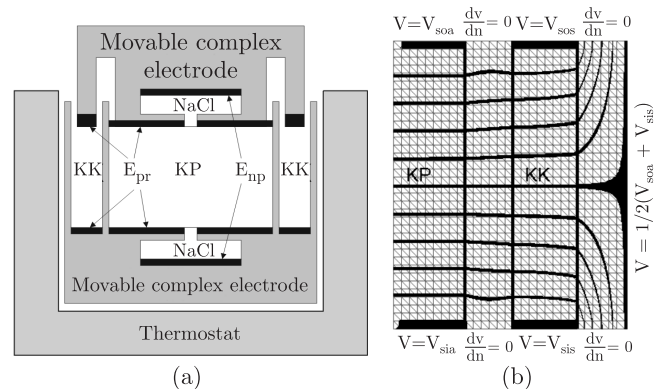


Fig. 2. a) A two-compartment cell for EI spectroscopy measurements; *KP* – measuring compartment, *KK*– correction compartment; the shield potential equal to the mean value of voltages between current electrodes  $E_{pr}$ ; (measurement voltage electrodes,  $E_{np}$ , are in contact with the tested tissue using an electrolytic bridge NaCl); b) electrical field distribution (owing to the symmetry only half the cell cross-section is presented);  $V_{soa}$ ,  $V_{sos}$ ,  $V_{sis}$ , voltage potentials of current electrodes in the compartments *KP* and *KK*;  $dV/dn = 0$  reflects the zero value of normal current density

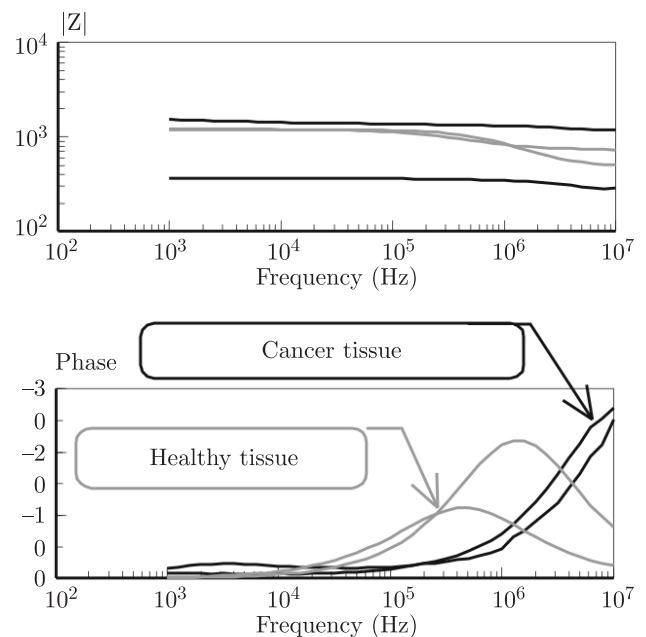
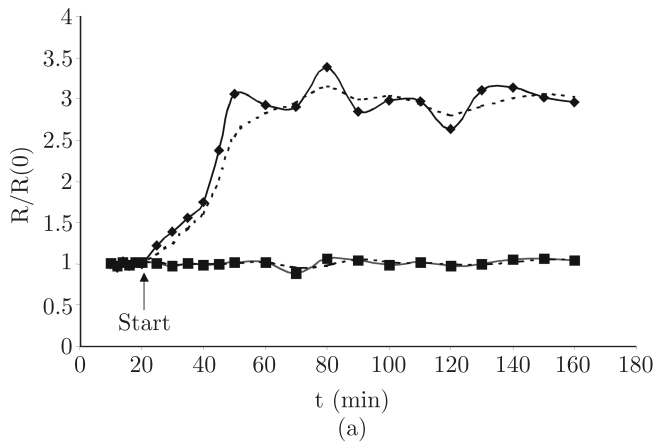


Fig. 3. Breast cancer tissue EI spectroscopy – measurement results



(b)

Fig. 4. Response to blood flow arrest: a) time course of the measured resistance (note that the resistance is referenced to the *resting* value  $R(0)$ ). Broken lines show the trend of the ratio  $R/R(0)$  measured in the affected and reference regions. The trend is calculated using a three-point moving average method with unequal weights, which is equivalent to low pass filtering, b) changes in the epicardium

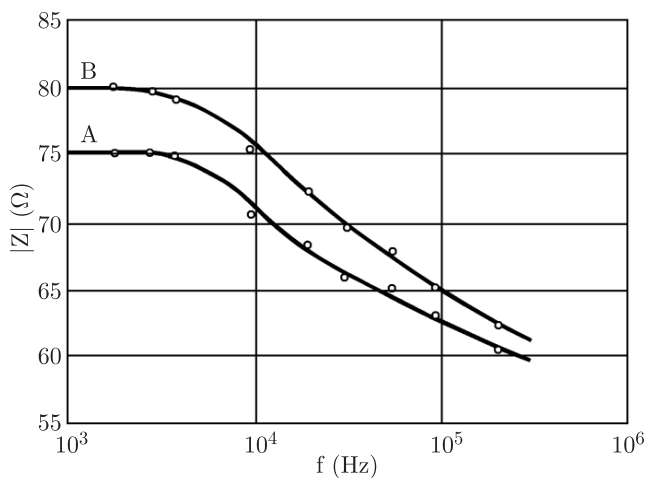


Fig. 5. The impedance modulus  $|Z|$  versus frequency  $f$  for an isolated rat heart: A – normal coronary perfusion B – perfusion with no oxygenated Krebs solution (hypoxaemia)

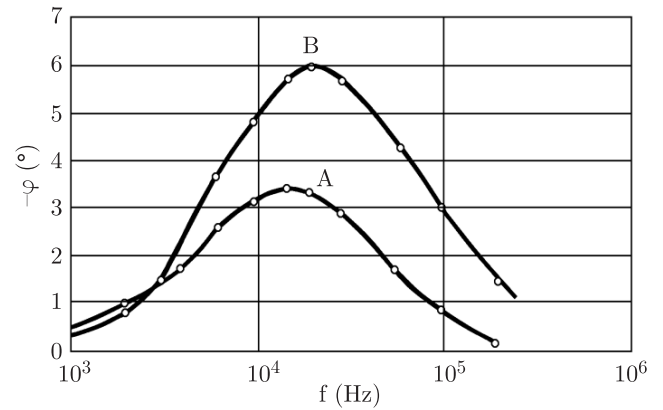


Fig. 6. The impedance phase angle  $\varphi$  versus frequency  $f$  for an isolated rat heart: A – normal coronary perfusion B – perfusion with no oxygenated Krebs solution (hypoxaemia)

detecting the impedance signal were placed between the current electrodes. The frequency was changed from 1.25 to 206 kHz. The results of an individual experiment are shown in Figs. 5 and 6. It is noticeable that an oxygen deficit in nutritive Krebs solution (hypoxaemia) causes an increase in the impedance modulus in the entire frequency range (Fig. 5) and also the maximum of the phase angle (Fig. 6).

#### 4. Impedance cardiography (ICG) and pletysmography (IPG)

Impedance cardiography, introduced by Kubicek et al [12] for the measurement of cardiac stroke volume, is based on a tetra-polar current method and a simplified model of the thorax. The traditional measurement of the electrical impedance modulus of a body segment, usually for a single frequency in the range 20–100 kHz, is widely used for the detection of respiration signals and for the evaluation of basic haemodynamic parameters, such as stroke volume, cardiac output, intervals of the cardiac cycle and limb blood flow. Selected clinical applications of impedance cardiography for systemic and pulmonary blood circulation are presented here. An application of particular note is the use of impedance pletysmography and cardiography for the examination of total systemic blood flow (SBF).

Several types of tetra-polar impedance rheographs, cardiographs and impedance spectrometers have been designed and applied in research work at the Institute of Precision and Biomedical Engineering of Warsaw University of Technology.

The rheograph was designed for the measurement and analysis of the impedance modulus ( $Z_0$ ) and its changes ( $\Delta Z$ ) in a chosen body segment or tissue area on the basis of the tetra-polar current method with simultaneous recording of the ECG signal. The instrument is equipped with a serial port RS232 and with a general purpose PC computer to control the system operation. The analogue part contains a current oscillator and impedance detection system. The voltage from the sinusoidal oscillator is fed at a frequency of 95 kHz to the current source, which provides high output impedance (over 100 k $\Omega$ ). This construction practically eliminates the influence of the electrode-tissue impedance and ensures constant amplitude, here set at the safe level of 1 mA. The selective amplifier

of high input impedance (over 200 kΩ) receives a signal from the detection electrodes. The signal from the selective amplifier, in amplitude proportional to the modulus of the measured impedance, is fed to a peak detector, which gives the voltage as the measure of  $Z_0$  in the range (4–40) Ω. This signal, after selective amplification within the frequency bandwidth 0.2–40 Hz, gives the component of an impedance change signal  $\Delta Z$  in the range 40–400 mΩ. A dedicated controller can control the amplitude of the  $\Delta Z$  signal digitally. For patient safety, an isolation barrier was developed to isolate the circuits in direct contact with the patients from the circuits co-operated with the computer or other peripheral devices. The digital part of the impedance rheograph is based on a micro-controller type 80C552 (Philips) that converts the analogue voltage signals ( $Z_0$ ,  $\Delta Z$ , ECG) into digital data.

The impedance rheographs was applied to clinical study, particularly for systemic and pulmonary blood flow assessment. The instrument, described more precisely in [21], was applied for the study of impedance spectral features of the tissues during their different states (for example during ischaemia).

**4.1. Study of systemic blood circulation.** For systemic blood flow (SBF) investigation an alternating current with an amplitude level of 1 mA and a frequency of about 100 kHz is injected longitudinally to the chest using two band electrodes around the upper part of neck or forehead and the waist

(Fig. 1b). The impedance signals are detected by two band or disc electrodes, one located around the neck base and the other around the thorax at the level of the xiphoid. This electrode set-up was used to determine stroke volume (SV) and total systemic blood flow (SBF).

The SV is calculated from the Kubicek formula as [12]:

$$SV = \rho \left( \frac{L}{Z_0} \right) \left| \frac{dZ}{dt} \right|_{\max} T, \quad (8)$$

where  $\rho$  – blood resistivity in Ωcm, calculated on the basis of haematocrit (Ht);  $\rho = 52.3 \times \exp(0.022 \times (\text{Ht}))$ ;  $L$  – distance between the detecting electrodes;  $Z_0$  – base impedance modulus;  $|dZ/dt|_{\max}$  – maximum value of the first derivative of the impedance change during the heart systole period;  $T$  – left ventricular ejection time. The SBF is determined by multiplication of an averaged value of  $SV$  taken from several cycles and the heart rate (HR).

The experimental and clinical findings show that the absolute value of the SV as determined by the impedance method is not accurate and in abnormal conditions, such as those created by certain cardiac defects or blood vessel abnormalities, the error in SV can exceed 20%. Nevertheless, the impedance method is very sensitive and fairly accurate for the observation of SV changes. In addition, the morphological changes in the impedance signal provide very important diagnostic information for monitoring the mechanical activity of the heart from beat to beat (Figs. 7 and 8).

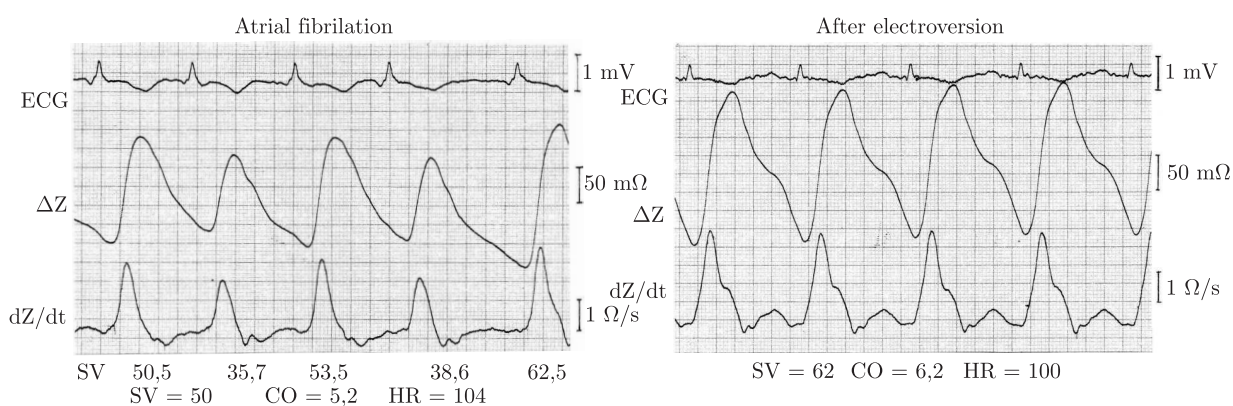


Fig. 7. ECG and ICG –  $\Delta Z$  and  $dZ/dt$  for a patient with atrial fibrillation (left) and after electroversion (right)

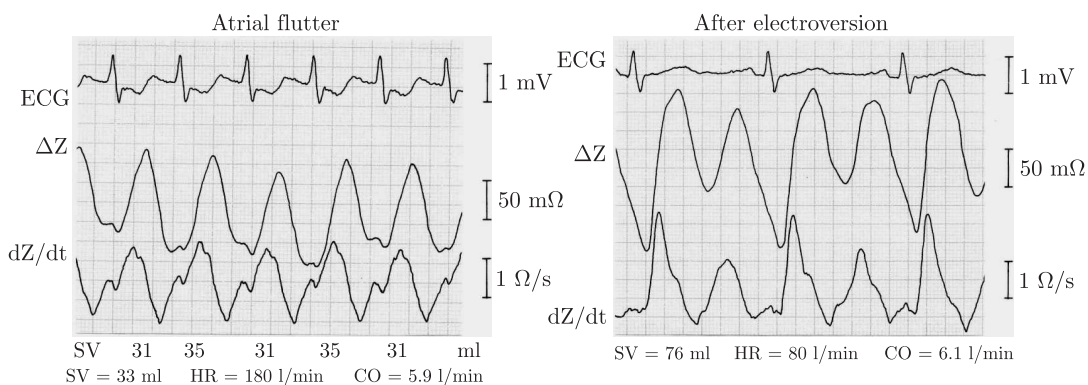


Fig. 8. ECG and ICG –  $\Delta Z$  and  $dZ/dt$  for a patient with atrial flutter (left) and directly after electroversion (right)

The investigations into SBF described in this study were carried out on 15 patients with cardiac arrhythmia, cardioverted electrically, including 14 patients with atrial fibrillation and one with atrial flutter. The results show that during atrial fibrillation the SV and HR fluctuated very distinctly from beat to beat but the CO averaged over 1 min was almost constant. The CO for different patients with atrial fibrillation varied from 3.2 l/min to 6.6 l/min and the mean CO for this group equalled about  $5.3 \pm 0.75$  l/min. After electroversion, all of these parameters (SV, HR and CO) appeared relatively stable and the CO was usually significantly higher than that during atrial fibrillation and fluctuated among the patients from 4.4 l/min to 7.0 l/min. The mean CO =  $5.9 \pm 0.68$  was about 12% greater than before cardioversion. Surprisingly, atrial flutter, even with a heart rate as high as 180 beats per minute, does not cause any distinct change in the CO in comparison with normal sinus rhythm after electroversion.

The investigation confirmed that atrial fibrillation causes different degrees of haemodynamic disorder. Restoration of the sinus rhythm from atrial fibrillation increases the CO significantly, in the range from about 5% to 30%, depending on the patient, usually higher than the value for a fast ventricle contraction rate, on average about 12%. This result is in agreement with [22], reporting that the absence of sinus rhythm causes a decrease in the CO from 7% to 25%

**4.2. Study of pulmonary blood circulation.** Our method [23,24], proposed for right pulmonary artery blood flow (RPABF) assessment is based on injection of an alternating current in the transversal direction to the thorax, on the right pulmonary artery level. This relates to the second intercostal space (2 ics) and a two-point detection of the voltage signal from the surface of the thorax in the same transversal direction and on the same level. Two band application electrodes of 5–10 cm in length are fixed around the hand or in the auxiliary middle line. Two typical disc electrodes for detection of an impedance signal are located along the right pulmonary artery on the 2 ics. One electrode is placed near the sternum and the second electrode is fixed in the right axillary line, on the same level. Thus, the direction of the current injection is the same as the direction of the blood flow through the right pulmonary artery and so is also the direction of signal detection (Fig. 9). Multiplication of the heart rate and part of the stroke volume determine the RPABF, which is calculated according to the Kubicek formula. The shape of the impedance signals (impedance change  $\Delta Z$  and the first derivative  $dZ/dt$ ) is also very important for diagnostic purposes (Fig. 10). The RPABF was studied on 20 healthy persons and 18 patients with Fallot Syndrome. The parameters examined differ significantly between healthy subjects and these patients. The RPABF calculated per square metre of body surface (RPABFi) appeared to be significant for recognition of pulmonary circulation abnormality. For healthy subjects  $RPABFi = 1.94 \pm 0.72$  l/min/m<sup>2</sup>, while for the patients  $SBFi = 1.12 \pm 0.41$  l/min/m<sup>2</sup>. The shape of impedance cardiographic curves also differs between healthy persons and the patients (Fig. 10).

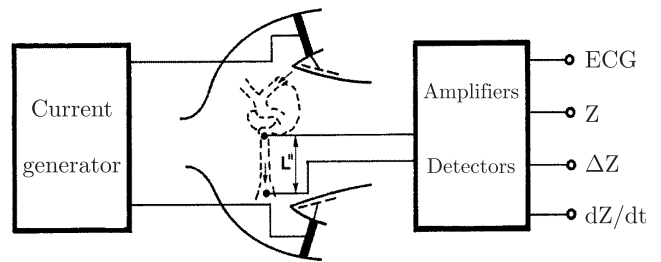


Fig. 9. The principle of right pulmonary artery blood flow (RPABF) examination

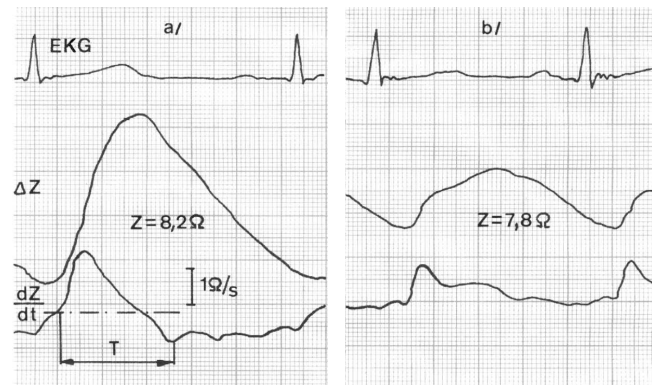


Fig. 10. Impedance cardiograms  $\Delta Z$  and  $dZ/dt$  with ECG for RPABF study: a) healthy subject, b) patient with Fallot Syndrome with pulmonary artery stenosis

**4.3. Clinical examination of human limb segments.** The investigations were performed on 6 patients with circulation disturbances (stenosis of the *arteria femoralis* and varicose veins) in a pelvic limb and 30 healthy persons as a reference group. The 2-minute arterial occlusion test in the pelvic limbs was additionally applied in healthy persons during impedance measurement. Two studies were performed with 10-minute arterial occlusion. For patients with circulation disturbances in one leg the impedance characteristics of the normal and abnormal limb (without occlusion) were compared. For the study of the spectral impedance characteristics of limb segments the commercial bioimpedance spectrometer type SEAC model SFB3 with a frequency range from 4 kHz to 1012 MHz was used. Examination of human limbs shows that spectral impedance characteristics in a patient with one normal and one abnormal leg (affected by circulation disturbances) are different (Figs. 11 and 12). In normal limbs no marked changes were observed during either the 2 or the 10-minute arterial occlusion in the limb. Thus, it can be concluded that the limb tissues are resistant and protected against disturbances of blood perfusion and the state of hypoxaemia. The extracellular to intracellular water ratio and membrane capacitance are also stable during the 10-minute arterial occlusion.

To conclude, the experiments on human limbs showed that the impedance equivalent scheme of the isolated rat heart and human limb segments, as for other biological tissues [10], could be presented as a parallel connection of extracellular fluid resistance and intracellular fluid resistance, serially connected with membrane capacitance.

It should be underlined, that the interpretation of ICG or IPG depends on several factors, which may be evidenced by careful analysis based on appropriate models of a tested organ. The basic factors which limit measurement accuracy are discussed elsewhere [7,25–27].

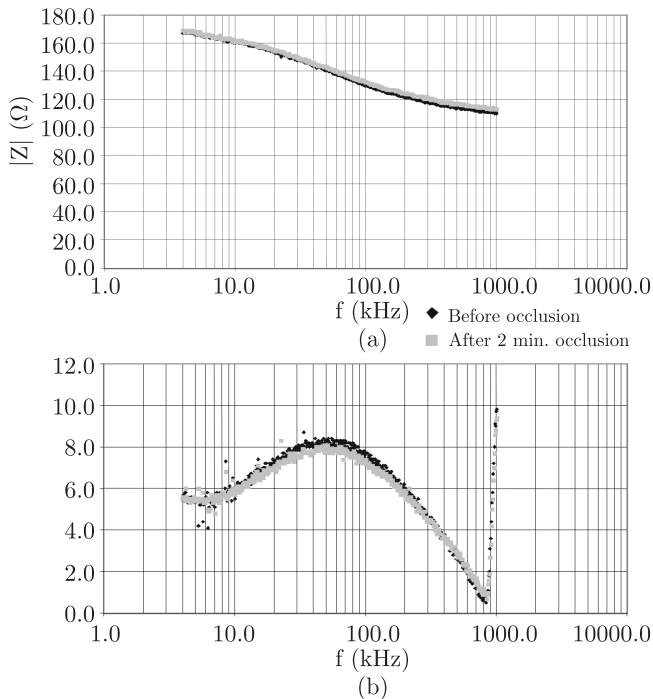


Fig. 11. The lower limb segment impedance modulus  $|Z_0|$  (a) and the phase angle  $\varphi$  (b) versus frequency  $f$  for a healthy person before and after the 2-minute occlusion

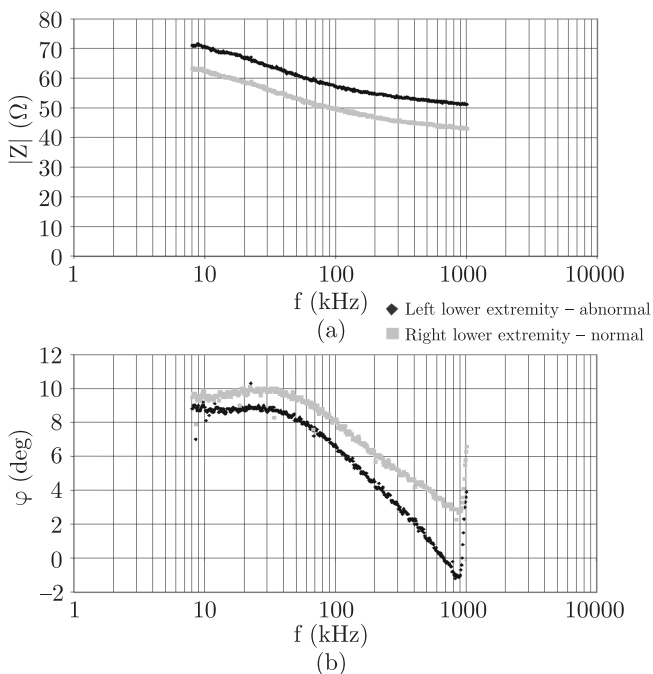


Fig. 12. The lower limb segment impedance modulus  $Z$  (a) and the phase angle  $\varphi$  (b) in versus frequency  $f$  for a patient with limb circulation disturbances (ischaemia and varicose veins)

## 5. Electrical impedance tomography (EIT)

The development of electrical impedance tomography (EIT) depends on advances in the modelling of the organs tested, on the development of reconstruction algorithms and on the construction of instrumentation allowing 2-D and 3-D measurements and analysis. The main advantages of this technology are the relatively low cost of instrumentation and its safety in operation, while the main disadvantages are the limited spatial and temporal resolutions of the method, depending on the limited number of electrodes applied and the limited resolution of the reconstruction algorithms.

The recognition of solid organs in EIT is not very difficult and measurement conditions present no great difficulty either. This is the reason why functional EIT systems based on 16/32 electrodes are already available. The situation is much more complicated in the case of organ visualisation if the tissue properties are not differentiated by orders of magnitude. This is typically the case in the recognition of tumours as in mammography. Here speed of operation is not so essential but spatial resolution and the differentiation of tissues at the very beginning of a malignant state is of the highest importance.

**5.1. Hardware.** On the basis of tissue spectroscopic measurements a suitable frequency or several frequencies of measurement signal may be proposed, allowing optimisation of the EIT instrumentation. The most evident is the great difference in permittivity between healthy and cancerous tissues, at higher frequencies of more than 1 MHz. However, the most important information for the use of EIT in mammography is that the region of changed electrical tissue properties is much more extensive than the region detected by any of the accessible visualisation techniques, including USG, MRI or X-ray mammography. This leads to the conclusion that EIT mammography is very promising for the early detection of breast cancer and for screening procedures. Several of our constructions and research on EIT are presented here [7,28–34].

In EIT the following problems of electrode construction are of the highest importance:

- accuracy of measurements; the material for the electrodes is important in avoiding high electrode impedance; separate tetra-polar electrodes should be applied;
- the size of the electrodes in terms of the density of the current applied to the object is limited and depends on frequency; the applied current density must be safe for a patient;
- the number of electrodes applied is directly responsible for the spatial resolution of an EIT system.

Assuming that, as is advisable, a set of combined electrodes of separate current and voltage elements allowing tetra-polar measurements are used, for a given number  $N$  of applied electrodes the number of independent measurements  $P$  is

$$P = \frac{N(N-1)}{2}, \quad (9)$$



giving only 120 independent measurements for 16, 2016 for 64 and 8128 for 128 electrodes. Theoretically the use of 16 electrodes should allow determination of around 1% of a tested 2-D surface, while in the case of 3-D the resolution for 128 electrodes should be around 0.01% of the space volume. In practice these values are at least one order of magnitude lower, because of the limited accuracy of individual measurements and the noise and quality of the reconstruction algorithms [29].

The locations of the electrodes and the applied measurement strategy are of great importance. For 2-D reconstruction this is usually a circular array of electrodes positioned in a plane around an object; for 3-D examples a cylinder or a hemisphere, with several rings of electrodes are usually applied. Application to the breast of two parallel plane electrode arrays seems to be an attractive solution for mammography, as it follows the practice of clinical X-ray mammography. As the measurement strategy, adjacent current excitation and voltage measurements on all other electrodes is possible. Another typical solution is polar excitation. The worst signal-to-noise ratio is in the first case and the best is for the polar excitation. Another possibility is excitation by a set of current patterns, which would maximise the signal-to-noise ratio (Adaptive Current Tomography proposed by Gisser in 1988 [35]).

The last hardware problem is related to the construction of front-ends, the sources of excitation – the current or voltage generators and fast acquisition systems. Recent work has concentrated on the introduction of the idea of multi-frequency measurements and direct readings of the characteristic differences that exist at different frequencies. Data acquisition systems (DAS) based on modern computer technology and using modern DSP systems are being developed. Measurement data are obtained from a number of versatile active electrodes (Fig. 13), which may be used either as a source of voltage or current excitation and as a current-voltage measurement device. This is a compact device as a result of the SMD technology applied [36].

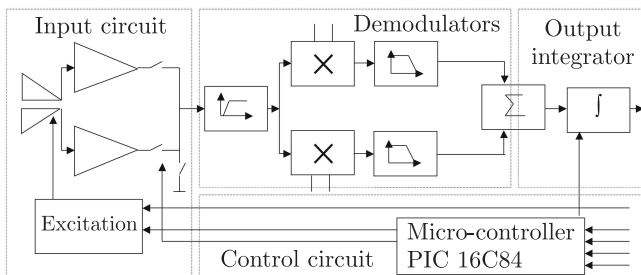


Fig. 13. Block diagram of an active compound electrode

**5.2. Image reconstruction.** In EIT the reconstruction of the absolute (AR) or relative (RR) properties of a tested structure is possible. RR algorithms are generally fast and of low computational cost but the results are not precise and therefore they are applied to solve qualitative problems, such as the functioning of organs. AR methods are based on iterative procedures and are much more precise but the computational cost is much higher than in the case of RR.

Kocikowski proposed a 3-D reconstruction algorithm for electrical impedance tomography [32] referred to as Regulated Correction Frequency Algebraic Reconstruction Tomography (RCFART) applied in GUT electrical impedance mammography [28,31]. The algorithm is a generalised form of the absolute reconstruction perturbation method with previously known algorithms, the SIRT (Simultaneous Iterative Reconstruction Technique) and the ART (Algebraic Reconstruction Technique), as limiting solutions methods [37,38]. It has a generic character and brings together the positive features of the previously known methods of ART and SIRT:

$$\forall_{\substack{h=1 \dots H \\ l=h+(j-1)H}} \Delta \alpha_e^{(h+1,j)} = \gamma \alpha_e^{(hi)} \frac{\sum_{j=1}^{L/H} \sum_{k=1}^K c_k^{(li)} S_{p(k,l)e}^{(i)}}{\sum_{j=1}^{L/H} \sum_{k=1}^K |S_{p(k,l)e}^{(i)}|} \quad (10)$$

$$\alpha_e^{(1,j+1)} \equiv \alpha_e^{(H+1,i)}$$

For a given iteration  $i$ , in the following corrections  $h = 1 \dots H$ , the admittivities  $\alpha_e$  of model elements are modified for sub-series  $L/H$  of regularly dispersed excitations  $l$ . For current distribution of conductivity  $\alpha_e^{(hi)}$  the corrections are proportional to normalised relative covariance deviations  $c_k^{(li)}$  of  $k$ -the measured and calculated currents for  $l$ -the excitation and sensitivity  $S_{p(k,l)e}^{(i)}$  of these measurements to the change of element  $e$  parameters. Current sensitivities are calculated for each of the iterations. Reconstruction process convergence depends on a value of the over-relaxation co-efficient  $\gamma$ . Correction frequency  $H$  should be a divisor of the number of excitations  $L$ .

SIRT and ART are specific singular cases of the RCFART algorithm for the extreme values –  $H = L$  for ART and  $H = 1$  for SIRT. For intermediate values one may expect the advantages of both methods – good stability and minor errors, as in SIRT, and fast convergence, as in ART.

Another approach is based on the application of different potential to the electrodes (in the simplest case potential is applied only to one selected electrode, while the other electrodes are connected to a common potential) and measuring the resulting current. An error function can be defined [7]:

$$\Phi(\sigma) = \sum_{j=1}^L \Phi_j \quad (11)$$

$$= \frac{1}{2} \sum_{j=1}^L (\mathbf{i}_j^0(\sigma) - \mathbf{i}_j^m)^T (\mathbf{i}_j^0(\sigma) - \mathbf{i}_j^m),$$

where  $\Phi(\sigma)$  is the global function of error,  $\Phi_j$  – error for the  $j^{\text{th}}$  projection,  $\mathbf{i}_j^0(\sigma)$  vector of the calculated currents resulting from  $j$ -th potential pattern,  $\mathbf{i}_j^m(\sigma)$  – vector of measured currents,  $L$  – number of projections (potential patterns).

$$\Delta \sigma^k = - \left\{ \mathbf{J}^T \mathbf{J} + [\mathbf{J}']^T [\mathbf{J} \otimes \mathbf{r}] \right\}^{-1} \mathbf{J}^T \mathbf{r}, \quad (12)$$

where  $\Delta \sigma^k$  – conductivity correction for  $i^{\text{th}}$  iteration,  $\otimes$  – Kronecker product,  $\mathbf{J}$  – Jacobian with entries defined as  $J_{ij} = \partial i_j^0 / \partial \sigma_j$ ,  $\mathbf{J}'$  – the derivative of Jacobian with respect to conductivity,  $\mathbf{I}$  – unit matrix, and residuum  $\mathbf{r} = \mathbf{i}^0(\sigma^k) - \mathbf{i}^m$ .

Table 1

Algorithm	Memory cost	Approximate calculation cost	Quality
back projection <sup>*1</sup>	$1.4P^{1/2}E$	$2.8P^{1/2}E + 0.285P^{1/2}E^{5/3}$	poor
SIRT <sup>2</sup>	$2PE$	$40EP + 0.285P^{1/2}E^{5/3} + 0.015E^{7/3}$	good
sensitivity method <sup>3</sup>	$2E^2$	$13E^3$	good
Gauss-Newton method <sup>2, 4</sup>	$2E^2$	$2E^2P + 8E^5/2$	good
Wexler double-constraint algorithm <sup>5</sup>		$6EP + 0.57P^{1/2}E^{5/3}$	unstable
optimal control algorithm <sup>*6,7</sup>	$2E^2 + 2PE$	$4E^2 + 8EP$	medium

<sup>1</sup>Barber [40]; <sup>2</sup>Yorkey [37]; <sup>3</sup>Murai [41]; <sup>4</sup>Cheney [42]; <sup>5</sup>Wexler [43]; <sup>6</sup>Marsili [44]; <sup>7</sup>Kozuoglu [45]; there are numerous other methods but these are less relevant to 3-D reconstruction.  $E$  – number of model elements;  $P$  – number of independent measurements;  $N$  – number of electrodes. Only multiplication and division are considered. It should be emphasised that different implementations have different calculation costs. There are also possible optimisations. The methods also differ in the number of iterations needed to obtain satisfactory results from reconstruction

Calculation of the Hessian is time-consuming and difficult. However, a close inspection of the relation reveals that the second part of the Hessian contains multiplication of the unit matrix and residuum. In the event of the residuum containing small values, this product can be omitted. Thus the starting value of conductivity and the resulting value of the residuum are the most important factors. The final form of the relation used in the reconstruction is

$$\sigma = \sigma_0 - \left[ \mathbf{J}^T \mathbf{J} + \lambda \cdot \text{diag} \left( \mathbf{J}^T \mathbf{J} \right) \right]^{-1} \mathbf{J}^T \mathbf{r}, \quad (13)$$

where  $\lambda$  is a regularisation co-efficient, calculated for an ill-conditioned problem. It can be evaluated using appropriate procedures. In our study by using diagonal matrix  $\text{diag} \left( \mathbf{J}^T \mathbf{J} \right)$  a constant value of  $\lambda$  was assumed.

Up to this point the above approach is similar to that proposed by Yorkey [39], although instead of potential, the current excitation pattern is here applied. An essential problem is the mode of Jacobian calculation. This is calculated using a so-called “complete electrode model” [7]. To solve the problem under discussion, the finite element method (FE) was used. The resulting equation is in the form  $\mathbf{i} = \mathbf{Y}\mathbf{V}$ , where  $\mathbf{Y}$  is the admittance matrix and vectors  $\mathbf{i}$  and  $\mathbf{V}$  contain node currents and potentials. The Jacobian entries are calculated using the relationship:

$$\frac{\partial i_{ei}}{\partial \sigma_j} = \int_{S_{el}} \frac{1}{z_{ei}} \mathbf{Y}_i^{-1} \frac{\partial \mathbf{Y}_i}{\partial \sigma_j} \mathbf{V} dS \quad (14)$$

where  $\mathbf{Y}_i$  – the admittance matrix for  $i$ -th projection;  $S_{el}$  – electrode surface,  $\sigma_j$  – conductivity of  $j$ -th element of the object,  $z_{ei}$  – characteristic impedance of the  $i$ -th electrode.

**5.3. Results.** In EIT the applied current flows in an unpredictable way and this is a serious problem resulting, for 2-D, in practical resolution of a 16-electrode system of about 12% of the image diameter. For full 3-D measurement and reconstruction using a 65-electrode system we have obtained around 0.5% volumetric resolution, which is far from the theoretical limit [28]. Table 1 shows the approximate cost of one iteration for the most important reconstruction methods applied in EIT [40–45].

Only AR methods may be precise enough for evaluation of tissue properties for EIT mammography (EIM). For 3-D cases the most important factor is the computational cost, as models are somewhat complex with a large number of components. Table 2 shows the cost of one iteration for three AR methods, for  $P = 2016$ ,  $N = 64$ ,  $E = 3824$  and  $W = 857$  ( $W$  – number of nodes), applicable to 3-D EIM mammography at Gdańsk University of Technology [28].

Table 2

Algorithm	Memory cost (in kilo cells)	Calculation cost (in kilo operations)
SIRT	15,418	323,764
Sensitivity method	29,246	726,937,000
Gauss-Newton method	29,246	66,194,000

Practically all experiments are studied, before practical implementation, using simulation methods. By these means the features of the RCFART algorithm have been extensively tested. An example of a hemispherical measuring head is shown in Fig. 14. In this kind of configuration the measuring head is unchangeable. To obtain a better resolution it is worth decreasing the volume inspected, as in traditional mammography, where two plates compress the breast.

Figure 15 presents an example of potential distribution inside a circular object containing four regions of conductivity different from the background and the result of reconstruction. Two FE models containing a different number of elements are used in the reconstruction process. The dense one is used in the so-called “forward problem” while the coarse one is used in the “inverse problem”. This allows more precise calculations to be made of the potential distribution inside the object and thus the current distribution. The initial value of conductivity  $\sigma_0$  is calculated from:

$$\sigma_0 = \frac{\sum_k \sum_l i_l^k i_l^k(1)}{\sum_k \sum_l [i_l^k(1)]^2}, \quad (15)$$

where  $i_l^k$  – measured current,  $i_l^k(1)$  current calculated for a uniform object of conductivity equal to 1.

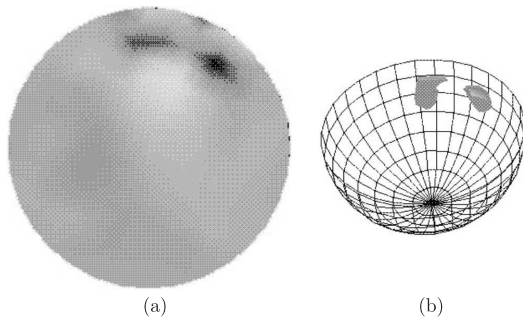


Fig. 14. Reconstruction of 3-D EIT measurements (left) and a filtered picture of higher conductivity components in the phantom (right)

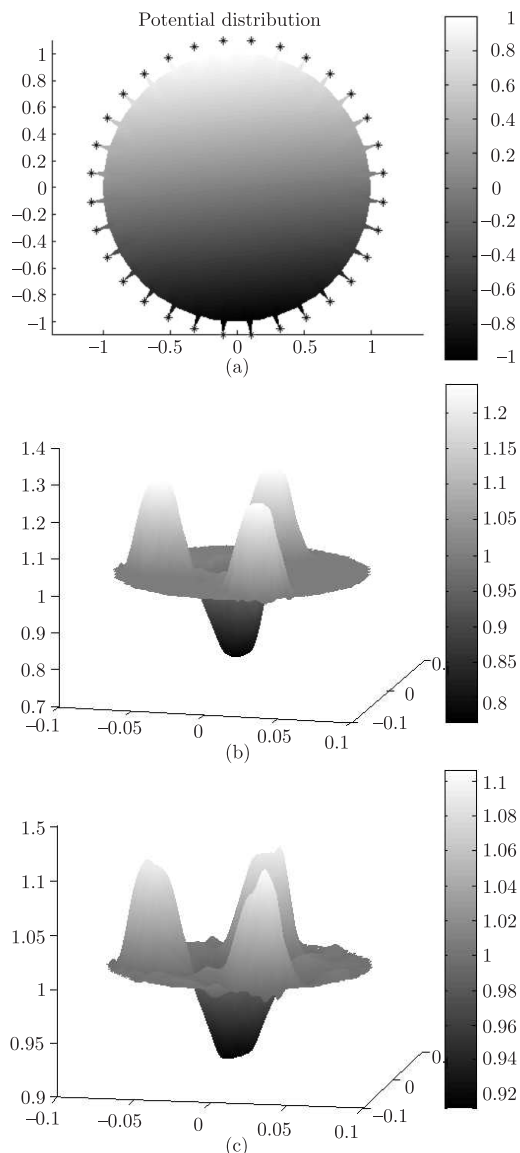


Fig. 15. a) Potential distribution inside the uniform object for the trigonometric (cosine) excitation pattern applied to the boundary; b) Actual conductivity distribution. Four perturbation of conductivity are respectively 1.2 S/m and 0.8 S/m. The conductivity of the background is 1 S/m; and c) reconstructed conductivity distribution inside the object after one iteration

This case is especially difficult to reconstruct as three regions of higher conductivity surround the region of lower conductivity. The difference between the actual and reconstructed values is clearly visible. However, only a few iterations are sufficient to achieve a sharp reduction in this discrepancy [46].

## 6. Conclusions

The methods presented are relatively inexpensive and easy to use in a number of medical applications, which constitute the main arguments for employing EI in clinical practice.

Impedance spectrometry is useful for the characterisation of tissues, allowing discrimination between normal and affected structures. Impedance spectral characteristics change during tissue hypoxaemia and blood flow arrest and many other cases may be effectively diagnosed.

Impedance cardiography methods for systemic and pulmonary blood circulation studies are extremely helpful, giving important diagnostic information. Cardiac output and the morphology of impedance signals differ significantly for healthy persons and patients with pathological circulation. There are other important applications too, such as IPG, recommended for the evaluation of peripheral blood flow and vascularisation.

EIT is still in the research phase, especially for the 3-D presentation of organs. Some applications are very useful and enable functional studies of organs to be performed, applicable, for example, to respiratory problems. Our results, with the discrimination of changed tissues at the relative volume of 1%, are still not sufficient for clinical applications in mammography. For 3-D EIT the sensitivity and resolution of absolute EIT needs to be improved. The fact that the technology seems to have properly matured for functional visualisation, as in cardiology or pulmonology for example, is a positive sign.

Rapid advances in electronic technology will probably ensure that future EI instrumentation will meet the requirements of such clinical applications as tissue discrimination for cancer detection or a more accurate study of the brain. Important improvements may be expected using differential multi-frequency measurements.

**Acknowledgements.** The authors extend their thanks to all their co-workers and Ph.D. students who participated in the development of the EI instrumentation and in the experiments and who produced some of the data presented. The participation of medical staff from the Department of Plastic Surgery and Burns Treatment and of Prof. J. Rogowski and Prof. J. Siebert from the Departments of Cardiac Surgery and Cardiology of Medical University of Gdańsk and others has been highly appreciated. The *in vivo* animal experiments were performed at the Department of Animal Physiology, Gdańsk University with the main assistance of Dr W. Stojek. Others are listed in the attached bibliography as co-authors of common publications. The work was supported by several grants from KBN (The Polish Ministry of Science and Information) including 3T11E01027 and partially supported by the project EU-REKA EI 2939 – CAVASCREEN.

## REFERENCES

- [1] *Proc. IX Int. Conference on Electrical Bio-Impedance*, [eds.] E. Gersing and M. Schaefer, ICP RBI, Heidelberg, 1995.
- [2] *Proc. X Int. Conference on Electrical Bio-Impedance*, [eds.] P. Riu, J. Rosell, R. Bragos, and O. Casas, Publ. Office of UPC, Barcelona, 1998.
- [3] *Proc. XI Int. Conference on Electrical Bio-Impedance*, [eds.] S. Grimnes, O. Martinsen, and H. Bruvold, Oslo, 2001.
- [4] *Proc. XII Int. Conference on Electrical Bio-Impedance*, [eds.] A. Nowakowski, J. Wtorek, A. Bujnowski, and A. Janczulewicz, Gdańsk, 2004.
- [5] P. Riu, J. Rosell, R. Bragos and O. Casas, "Electrical bioimpedance methods", *Ann. NY Acad. Sci.* 873, (1999).
- [6] J.P. Morucci, M.E. Valentinuzzi, B. Rigaud, C.J. Felice, N. Chauveau, and P.M. Marsili, "Bioelectrical impedance techniques in medicine", *Crit. Rev.<sup>TM</sup> in Biomed. Eng.* 24(4-6), 223-681 (1996).
- [7] J. Wtorek, *Electroimpedance Techniques in Medicine*, GUT Publ., Monograph series: 43, 2003, (in Polish).
- [8] *Physiological Measurement*, [eds.] R.H. Bayford, A. Nowakowski, 26(2), 2005.
- [9] J. Wtorek, A. Nowakowski, T. Pałko, and W.G. Pawlicki, "Bioelectroimpedance measurements", in *Biocybernetics and Biomedical Engineering 2000* 2, 477-512 (2001), (in Polish).
- [10] T. Pałko, B. Galwas, and G. Pawlicki, "Passive electric tissue properties and applications", in *Biocybernetics and Biomedical Engineering 2000* 9, 363-400 (2002), (in Polish).
- [11] J. Wtorek, A. Nowakowski, A. Bujnowski, and J. Siebert, "Electroimpedance tomography", in *Biocybernetics and Biomedical Engineering 2000* 8, 697-758 (2003), (in Polish).
- [12] W.G. Kubicek, J.R. Karnegis, R.P. Patterson, D.A. Witose, and R.H. Mattson, "Development and evaluation of an impedance cardiographic system to measure cardiac output and other cardiac parameters", *Aerospace Medicine* 37, 1208-1212 (1966).
- [13] D.B. Geselowitz, "An application of electrocardiographic lead theory to impedance plethysmography", *IEEE Trans. Biomed. Eng.* 18, 38-41 (1971).
- [14] J. Wtorek, A. Polinski, J. Stelter, and A. Nowakowski, "Cell for measurements of biological tissue complex conductivity", *Technology and Health Care* 177-193, (1998).
- [15] J. Wtorek, L. Józefiak, A. Poliński, and J. Siebert, "An Averaging Two-Electrode Probe for Monitoring Changes in Myocardial Conductivity Evoked by Ischemia", *IEEE Trans. Biomed. Eng.* 49(3), 240-246 (2002).
- [16] J. Wtorek, A. Bujnowski, A. Poliński, L. Józefiak, and B. Truyen, "A Probe for Immittance Spectroscopy Based on the Parallel Electrode Technique", *Physiol. Meas.* 25(5), 1249 - 1260 (2004).
- [17] J. Stelter, J. Wtorek, A. Nowakowski, A. Kopacz, and T. Jastrzębski, "Complex permittivity of breast tumour tissue", *Proc. of X<sup>th</sup> ICEBI*, Barcelona, Spain, 59-62, (1998).
- [18] J. Wtorek, A. Bujnowski, A. Poliński, and A. Nowakowski, "A six-ring probe for monitoring conductivity changes", *Physiol. Meas.* 26(2), S69-S79 (2005).
- [19] J. Wtorek and A. Poliński, "The contribution of blood-flow-induced conductivity changes to measured impedance", *IEEE Trans. on Biomed. Eng.* 52, 41-49 (2005).
- [20] J. Siebert, J. Wtorek, and J. Rogowski, "Stroke volume variability - cardiovascular orthostatic manoeuvre in patients with coronary artery diseases", *Ann. NY Acad. Sci.* 873, 182-190 (1999).
- [21] T. Palko, F. Bialokoz, and J. Weglarz, "Multifrequency device for measurement of complex electrical bio-impedance-design and application", *Proc. RC IEEE - EMBS & 14<sup>th</sup> BMESI*, 87-94 (1995).
- [22] H. Kanai, "Frequency characteristics of electrical properties of living tissues and its clinical applications", *Proc. VIII<sup>th</sup> ICEBI*, Kuopio, 5-7, (1992).
- [23] T. Palko and B. Szafjanski, "Analysis of possibilities of a quantitative estimation of pulmonary blood flow by an impedance rheographic method", *Probl. Med. Techn.* 15, 33-42 (1984), (in Polish).
- [24] T. Palko, "Rheoimpedance methods for aortic and pulmonary blood flow", *Med. Biol. Eng. Comp.* 23, Suppl. 1, 119 (1985).
- [25] J. Wtorek, A. Poliński, and J. Siebert, "Influence of spatial conductivity distribution on relative contributions to ICG signals from thorax - FEM model study", *IEEE Engineering in Medicine and Biology Society, 18<sup>th</sup> Ann. Intern. Conf.*, CD-ROM-933, Amsterdam, 1996.
- [26] A. Poliński, J. Wtorek, A. Nowakowski, and L. Józefiak, "Anisotropy in impedance plethysmography", *Proc. of 4<sup>th</sup> Europ. Conf. on Eng. & Med.*, Warsaw, 15-16 (1997).
- [27] J. Wtorek, "Relations between components of impedance cardiogram analyzed by means of finite element model and sensitivity theorem", *Ann. Biomed. Eng.* 28 (11), 1301-1310 (2000).
- [28] A. Nowakowski, J. Wtorek, and J. Stelter, "Technical University of Gdańsk Electroimpedance mammography", *IX ICEBI*, Heidelberg, 434-437, (1995).
- [29] M. Kocikowski, A. Poliński, A. Nowakowski, and J. Wtorek, "Problems of 3D reconstruction and visualisation in EIT", *Task Quarterly* 1 (2), 162-174 (1997).
- [30] J. Wtorek, J. Stelter, and A. Nowakowski, "Impedance mammograph 3D phantom studies", *Ann. NY Acad. of Sci.* 873, 520-533 (1999).
- [31] A. Nowakowski, J. Wtorek, A. Bujnowski, J. Stelter, A. Hahn, and A. Mączynski, "Dual frequency 128 electrode electroimpedance tomograph (DFEIT)", European Medical & Biological Engineering Conference, *Medical & Biological Engineering & Computing incorporating Cellular Engineering* 37, Suppl. 2, 156-157, (1999).
- [32] M. Kocikowski and A. Nowakowski, RCFART - 3D Reconstruction Algorithm for EIT, *Proc. of X<sup>th</sup> ICE BI*, Barcelona, 425-428, (1998).
- [33] A. Bujnowski and J. Wtorek, "Comparison of the current-mode back projection and Jacobian-based reconstruction algorithms", *Proc. XII ICEBI & V EIT*, Gdańsk, 599-602 (2004).
- [34] A. Bujnowski, J. Wtorek, and B. Truyen, "Modular impedance tomograph for shallow soil subsurface investigations", *Proc. XII<sup>th</sup> ICEBI & V<sup>th</sup> EIT*, Gdańsk, 665-668 (2004).
- [35] G. Gisser, D. Isaacson, and J. Newell, "Theory and performance of an adaptive current tomography", *Clin. Phys. Physiol. Measur.* 9, suppl. A, 35-41 (1988).
- [36] J. Wtorek, A. Bujnowski, J. Stelter, and A. Nowakowski, "Algorithm and the circuit for measurements in EIT", Patent 331130/1999.01.29, (in Polish).
- [37] T.J. Yorkey, J.G. Webster, and W.J. Tompkins, "An improved perturbation technique for electrical impedance imaging with some criticism", *IEEE Trans. on Biomed. Eng.* 34, 898-901 (1987).
- [38] Y. Kim, J.G. Webster, and W. J. Tompkins, "Electrical impedance imaging of the thorax", *J. Microwave Power* 18, 245-257 (1983).

- [39] T.J. Yorkey, J.G. Webster, and W.J. Tompkins, "Comparing reconstruction algorithms for electrical impedance tomography", *IEEE Trans. on Biomed. Eng.* 34, 843–852 (1987).
- [40] D.C. Barber and B.H. Brown, "Recent developments in applied potential tomography", *Processing in Medical Imaging*, [ed.] Bacharach, 106–1211 (1986).
- [41] T. Murai and Y. Kagawa, "Electrical impedance computed tomography based on a finite element model", *IEEE Trans. Biomed. Eng.* 32, 177–184 (1985).
- [42] M. Cheney, D. Isaacson, J. Newell, J. Globe, and S. Simske, "NOSER: An algorithm for solving the inverse conductivity problem", *Int. J. Imaging Systems Technology* 2, 66–75 (1990).
- [43] A. Wexler, B. Fry, and M.R. Neiman, "Impedance-computed tomography algorithm and system", *Appl. Opt.* 24, 3985–3992 (1985).
- [44] P.M. Marsili, V. Amalric, G. Mounie, M. Granie, and J.P. Morucci, "Optimal control and boundary element methods as a reconstruction algorithm in impedance imaging", *Proc. of a Meeting on Electrical Impedance Tomography*, Copenhagen, 116–127 (1990).
- [45] M. Kozuoglu, K. Leblebicioglu, and Y.Z. Ider, "A fast image reconstruction algorithm for electrical impedance tomography", *Physiol. Meas.* 15, A115–A124 (1994).
- [46] A. Janczulewicz and J. Wtorek, "An EIT reconstruction algorithm: a comparison of one-step and iterative versions", *Proc. SPIE* 5505, 144–150 (2004).